# GRAPH FILTERING FOR HUB NODE IDENTIFICATION IN BRAIN NETWORKS

Duc Vu, Meiby Ortiz-Bouza and Selin Aviyente

Department of Electrical and Computer Engineering, Michigan State University, East Lansing, MI

# ABSTRACT

Over the past two decades, complex network theory has been used to model both the functional and structural connectivity of the brain. Different graph theoretic metrics have been used to characterize the topology of brain networks. One important characteristic of brain networks is the existence of hub nodes, which are central to neural integration. Previous methods for hub node identification are primarily based on computing the centrality of the nodes based on the functional connectivity network. However, these approaches to hub identification may identify portions of large brain systems rather than critical nodes of brain networks. In this paper, we introduce an alternative view of hub nodes utilizing both the functional connectivity network and the neurophysiological signals defined on the nodes of this network. An unsupervised learning method is proposed to learn a graph filter that separates the hub nodes from normal nodes, where the hub nodes are defined based on the homophily of a node with respect to its neighbors. A metric to quantify the local total variation is introduced to identify the possible hub nodes. The proposed method is applied to electroencephalogram (EEG) data collected from a study of error monitoring in the human brain. The detected hub nodes are compared to existing methods.

*Index Terms*— Electroencephalogram (EEG), functional connectivity, graph signal processing, hub node, graph filtering

## 1. INTRODUCTION

In the past two decades, the field of complex networks has emerged as a powerful tool to characterize the structure and function of the human brain using a variety of tools from graph theory and network science [1]. In this line of research, the nodes of the network correspond to the different brain regions and the edges correspond to the structural or functional connectivity. Functional connectivity networks (FCNs) have been constructed from different modalities including EEG, MEG and fMRI, where the edges correspond to the pairwise similarity between the neurophysiological signals from different regions.

One of the key features of functional connectivity networks is the identification of hub nodes [2, 3]. Hubs are nodes with many edges or with edges that place them in central positions for facilitating information flow in a network. Hubs have been shown to be central in brain communication and neural integration and participate widely across a diverse set of cognitive functions [4]. The high level of centrality of brain hubs also renders them points of vulnerability that are susceptible to disconnection and dysfunction in brain disorders. Given the importance of hubs to network topology, the locations and functions of hubs in the brain are of paramount interest to neuroscientists. The most commonly used metrics for identifying hub nodes are the node degree, also known as degree centrality,

eigenvector centrality, closeness centrality and betweenness centrality [4]. Prior research has shown that degree-based approaches to hub identification are biased towards large brain systems rather than critical nodes of brain networks [3]. Moreover, these methods only rely on the functional connectivity network without considering the neurophysiological signals recorded on the nodes of this network.

Recently, tools from the field of graph signal processing (GSP) have been adapted to analyze brain signals with respect to the connectivity graphs they reside on [5]. Concepts of graph Fourier transform (GFT) and the corresponding notions of graph frequency components and graph filters have been utilized to analyze brain signals. These GSP tools permit the decomposition of a graph signal into different frequency components that represent different levels of variability and have been used for analyzing structural-functional coupling, dimensionality reduction, and classification [5, 6, 7]. Inspired by these advances, in this paper we propose to identify the hub nodes from the perspective of GSP, in particular using the concepts of low and high graph frequency. In this work, we will define hub nodes from the perspective of node homophily, i.e., nodes with similar features tend to connect with one another. Hub nodes may differ from their neighbors both in terms of their connectivity profile and their signal value, thus having higher frequency content compared to normal nodes. In recent years, graph neural networks (GNNs) have been leveraged for various graph learning tasks including outlier (anomaly) detection [8, 9]. However, recent studies [10, 11] indicate that most GNN models are not suitable for anomaly detection as they force the representation of neighboring nodes to be similar making the decision boundary between the normal and anomalous classes closer. Moreover, most of the GNN-based node classification methods are supervised or semi-supervised which makes them unsuitable for hub node identification in FCNs as there is no label information for hub nodes.

In this paper, we introduce an unsupervised graph signal processing based approach for identifying hub nodes in FCNs. The proposed approach is based on designing a graph filter for detecting hub nodes with the following assumptions: (i) hub nodes are sparse and heterophilic (high frequency/nonsmooth), i.e., have a more diverse set of connections, and (ii) the optimally filtered graph signal is homophilic (low frequency/smooth) with respect to the graph. A hub scoring function based on the local gradient of the nodes is also introduced. In this paper, we evaluate the proposed method on identifying the hub nodes in FCNs constructed from electroencephalogram (EEG) data, where the FCNs are constructed using the pairwise phase synchrony and the graph signals (attributes) are the EEG amplitudes. In particular, we identify the hub nodes following an error response in a Flanker task.

## 2. BACKGROUND

## 2.1. Functional Connectivity Networks

In this paper, reduced interference Rihaczek (RID-Rihaczek) time-frequency phase synchrony is used to quantify the functional con-

This work was supported in part by the NSF under CCF-2211645 and CCF-2312546.

nectivity between two brain regions [12]. For a signal  $x_i(t)$ , the RID-Rihaczek distribution is defined as [12]:

$$C_{i}(t,f) = \int_{-\infty}^{\infty} \int_{-\infty}^{\infty} e^{-\frac{(\theta\tau)^{2}}{\sigma}} e^{j\frac{\theta\tau}{\sigma}} A(\theta,\tau) e^{-j(\theta t + 2\pi f\tau)} d\tau d\theta, \quad (1)$$

where  $e^{-\frac{(\theta au)^2}{\sigma}}$  is the Choi-Williams kernel [13],  $e^{j\frac{\theta au}{\sigma}}$  is the kernel function for the Rihaczek distribution [14], and  $A(\theta, au)$  is the ambiguity function defined as  $A(\theta, au) = \int_{-\infty}^{\infty} x_i (u + \frac{ au}{2}) x_i^* (u - \frac{ au}{2}) e^{j\theta u} du$ .

From this complex distribution, one can obtain the instantaneous phase,  $\phi_i(t,f)$ , and the phase difference between two signals  $x_i$  and  $x_j$  as  $\phi_{i,j}(t,f) = \arg\left[\frac{C_i(t,f)C_j^*(t,f)}{|C_i(t,f)||C_j(t,f)|}\right]$ . Phase Locking Value (PLV), which quantifies the phase synchrony between  $x_i$  and  $x_j$ , is defined as the consistency of the phase differences across trials and can be computed as:

$$PLV_{i,j}(t,f) = \frac{1}{R} \left| \sum_{r=1}^{R} \exp\left(j\phi_{i,j}^{r}(t,f)\right) \right|, \tag{2}$$

where R is the total number of trials and  $\phi^r_{i,j}(t,f)$  is the phase difference for the rth trial. Once the pairwise PLV values are computed between all pairs of electrodes, the weighted adjacency matrix corresponding to the FCN can be constructed as the average of  $PLV_{i,j}(t,f)$  within the time interval and frequency band of interest.

## 2.2. Graphs

A graph  $\mathcal{G}=(V,E,\mathbf{A})$  is defined by a node set V with |V|=N, an edge set E and the adjacency matrix  $\mathbf{A}\in\mathbb{R}^{N\times N}$ . The graph Laplacian is given by  $\mathbf{L}=\mathbf{D}-\mathbf{A}$ , where  $\mathbf{D}$  is the diagonal degree matrix defined as  $\mathbf{D}_{ii}=\sum_{j}\mathbf{A}_{ij}$ . The normalized Laplacian matrix  $\mathbf{L}_n$  is defined as  $\mathbf{L}_n=\mathbf{D}^{-1/2}(\mathbf{D}-\mathbf{A})\mathbf{D}^{-1/2}=\mathbf{I}_N-\mathbf{D}^{-1/2}\mathbf{A}\mathbf{D}^{-1/2}=\mathbf{I}_N-\mathbf{A}_n$ , where  $\mathbf{I}_N$  is the identity matrix of size N and  $\mathbf{A}_n$  is the normalized adjacency matrix. The spectrum of  $\mathbf{L}_n$  is composed of the diagonal matrix of the eigenvalues,  $\mathbf{A}=diag(\lambda_1,\ldots,\lambda_N)$  with  $\lambda_1\leq\lambda_2\leq\ldots\leq\lambda_N$ , and the eigenvector matrix  $\mathbf{U}=[u_1|u_2|\ldots|u_N]$  such that  $\mathbf{L}_n=\mathbf{U}\mathbf{\Lambda}\mathbf{U}^{\top}$ .

# 2.3. Graph Filtering

A polynomial graph filter is described as the linear operator

$$\mathcal{H}(\mathbf{L}) = \sum_{t=0}^{T-1} h_t \mathbf{L}^t = \mathbf{U} \left( \sum_{t=0}^{T-1} h_t \mathbf{\Lambda}^t \right) \mathbf{U}^{ op},$$

where T is the filter order and  $h_t$ 's are the filter coefficients. The filtered graph signal  $\tilde{\mathbf{F}}$  is computed as  $\tilde{\mathbf{F}} = \mathcal{H}(\mathbf{L})\mathbf{F} = \mathbf{U}\mathcal{H}(\mathbf{\Lambda})\mathbf{U}^{\top}\mathbf{F}$ , where  $\mathcal{H}(\mathbf{\Lambda}) = \mathrm{diag}(\mathcal{H}(\lambda_1), \dots, \mathcal{H}(\lambda_N))$ .

Following the definitions in [15], we can define the t-th shifted input signal as  $\mathbf{S}^{(t)} := \mathbf{U}\Lambda^t\mathbf{U}^{\top}\mathbf{F}$ .  $\mathbf{S}_{(i)}$  can then be defined as a  $T \times P$  matrix corresponding to the i-th node where each row corresponds to the t-th shifted input signal at the i-th node with  $[\mathbf{S}_{(i)}]_t := [\mathbf{S}^{(t)}]_{(i)}$ .  $\tilde{\mathbf{F}}$  can the be rewritten as

$$\tilde{\mathbf{F}} = \mathbf{U} \left( \sum_{t=0}^{T-1} h_t \Lambda^t \right) \mathbf{U}^{\top} \mathbf{F} = \sum_{t=0}^{T-1} h_t \mathbf{S}^{(t)}.$$

Hence, the filtered graph signal corresponding to the i-th node can be computed as  $\tilde{\mathbf{F}}_i = \sum_{t=0}^{T-1} h_t[\mathbf{S}^{(t)}]_i = \mathbf{h}^{\top}\mathbf{S}_{(i)}$ . The p-th column of  $\mathbf{S}_{(i)}$  can be denoted as a T-dimensional vector,  $\mathbf{s}_i^p$ .

# 3. OPTIMAL GRAPH FILTERING FOR HUB NODE IDENTIFICATION (GRAFHUB)

#### 3.1. Problem Formulation

Given a graph with adjacency matrix  $\mathbf{A} \in \mathbb{R}^{N \times N}$ , and graph signal  $\mathbf{F} \in \mathbb{R}^{N \times P}$ , in this paper we focus on the detection of outliers or hubs, where the outliers are assumed to be high frequency and sparse compared to normal activity [16, 11]. The graph signal  $\mathbf{F}$  can be decomposed as  $\mathbf{F}_l + \mathbf{F}_h$ , where  $\mathbf{F}_l$  and  $\mathbf{F}_h$  are the low- and high-frequency parts, respectively. The goal is to learn a graph filter such that the filtered signal,  $\tilde{\mathbf{F}}$ , corresponds to the low-frequency activity which is smooth with respect to the underlying graph structure. This aim is formulated through the following cost function:

$$\alpha ||\mathbf{F} - \tilde{\mathbf{F}}||_1 + \operatorname{tr}(\tilde{\mathbf{F}}^{\top} \mathbf{L} \tilde{\mathbf{F}}),$$
 (3)

where the first term corresponds to the sparsity of the outliers and the second term quantifies the smoothness (graph total variation) and  $\alpha$  controls the tradeoff between these two terms. Expressing the filtered signal as  $\mathbf{U}\mathcal{H}(\mathbf{\Lambda})\mathbf{U}^{\top}\mathbf{F}$ , the objective function becomes

$$\min_{\mathbf{h}, \mathbf{h}^{\top} \mathbf{h} = 1} \quad \alpha || \mathbf{F} - \mathbf{U} \left( \sum_{t=0}^{T-1} h_t \mathbf{\Lambda}^t \right) \mathbf{U}^{\top} \mathbf{F} ||_1 
+ \operatorname{tr} \left( \mathbf{F}^{\top} \mathbf{U} \left( \sum_{t=0}^{T-1} h_t \mathbf{\Lambda}^t \right) \mathbf{U}^{\top} \mathbf{L} \mathbf{U} \left( \sum_{t=0}^{T-1} h_t \mathbf{\Lambda}^t \right) \mathbf{U}^{\top} \mathbf{F} \right),$$
(4)

where  $\mathbf{h} = [h_1, h_2, \cdots, h_{T-1}]$  is the vector of normalized polynomial filter coefficients.

## 3.2. Optimization

The proposed objective function is solved using ADMM [17]. By introducing an auxiliary variable  $\mathbf{Z} = \mathbf{F} - \mathbf{U} \left( \sum_{t=0}^{T-1} h_t \mathbf{\Lambda}^t \right) \mathbf{U}^{\top} \mathbf{F}$ , the optimization problem can be rewritten as

$$\min_{\mathbf{h}, \mathbf{Z}} \operatorname{tr} \left( \mathbf{F}^{\top} \mathbf{U} \left( \sum_{t=0}^{T-1} h_t \mathbf{\Lambda}^t \right) \mathbf{U}^{\top} \mathbf{L} \mathbf{U} \left( \sum_{t=0}^{T-1} h_t \mathbf{\Lambda}^t \right) \mathbf{U}^{\top} \mathbf{F} \right) 
+ \alpha ||\mathbf{Z}||_1, \text{ s.t } \mathbf{h}^{\top} \mathbf{h} = 1, \mathbf{Z} = \mathbf{F} - \mathbf{U} \left( \sum_{t=0}^{T-1} h_t \mathbf{\Lambda}^t \right) \mathbf{U}^{\top} \mathbf{F}.$$
(5)

The corresponding scaled augmented Lagrangian is

$$\mathcal{L}(\mathbf{Z}, \mathbf{h}, \mathbf{V}) = \operatorname{tr}(\mathbf{F}^{\top} \mathbf{U} \left( \sum_{t=0}^{T-1} h_t \mathbf{\Lambda}^t \right) \mathbf{U}^{\top} \mathbf{L} \mathbf{U} \left( \sum_{t=0}^{T-1} h_t \mathbf{\Lambda}^t \right) \mathbf{U}^{\top} \mathbf{F})$$
$$+ \alpha ||\mathbf{Z}||_1 + \frac{\rho}{2} ||\mathbf{Z} - (\mathbf{F} - \mathbf{U} \left( \sum_{t=0}^{T-1} h_t \mathbf{\Lambda}^t \right) \mathbf{U}^{\top} \mathbf{F}) + \mathbf{V}||_F^2,$$

where  $\mathbf{V} \in \mathbb{R}^{N \times P}$  is the Lagrange multiplier. **1.**  $\mathbf{Z}$  update: The variable  $\mathbf{Z}$  can be updated as

$$\mathbf{Z}^{k+1} = \underset{\mathbf{Z}}{\operatorname{argmin}} \ \mathcal{L}(\mathbf{Z}, \mathbf{h}^{k}, \mathbf{V}^{k}),$$

$$= \underset{\mathbf{Z}}{\operatorname{argmin}} \ \alpha ||\mathbf{Z}||_{1} + \frac{\rho}{2} ||\mathbf{Z} - (\mathbf{F} - \left(\sum_{t=0}^{T-1} h_{t}^{k} \mathbf{L}^{t}\right) \mathbf{F}) + \mathbf{V}||_{F}^{2},$$

$$= S_{\frac{\alpha}{\rho}} (\mathbf{F} - \mathbf{U} \left(\sum_{t=0}^{T-1} h_{t}^{k} \mathbf{\Lambda}^{t}\right) \mathbf{U}^{\top} \mathbf{F} - \mathbf{V}^{k}),$$
(6)

where  $S_{\alpha/\rho}(\cdot)$  is the elementwise thresholding operator which is the proximal operator of  $\ell_1$  norm [17].

2. h update: The filter coefficients h can be updated using:

$$\mathbf{h}^{k+1} = \underset{\mathbf{h}, \mathbf{h}^{\top} \mathbf{h} = 1}{\operatorname{argmin}} \mathcal{L}(\mathbf{Z}^{k+1}, \mathbf{h}, \mathbf{V}^{k}),$$

$$= \underset{\mathbf{h}, \mathbf{h}^{\top} \mathbf{h} = 1}{\operatorname{argmin}} \frac{\rho}{2} ||\mathbf{Z}^{k+1} - \mathbf{F} + \mathbf{U} \left( \sum_{t=0}^{T-1} h_{t} \mathbf{\Lambda}^{t} \right) \mathbf{U}^{\top} \mathbf{F} + \mathbf{V}^{k} ||_{F}^{2}$$

$$+ \operatorname{tr} \left( \mathbf{F}^{\top} \mathbf{U} \left( \sum_{t=0}^{T-1} h_{t} \mathbf{\Lambda}^{t} \right) \mathbf{U}^{\top} \mathbf{L} \mathbf{U} \left( \sum_{t=0}^{T-1} h_{t} \mathbf{\Lambda}^{t} \right) \mathbf{U}^{\top} \mathbf{F} \right). \quad (7)$$

Writing the terms in (7) as an elementwise multiplication, we have

$$\frac{\rho}{2} \sum_{p=1}^{P} \sum_{i=1}^{N} ((Z_{ip} - F_{ip} + \tilde{F}_{ip}) + V_{ip})^2 + \sum_{p=1}^{P} \sum_{i,j=1}^{N} \tilde{F}_{pi} L_{ij} \tilde{F}_{jp}.$$

Since  $\tilde{\mathbf{F}}_i = \mathbf{h}^{\top} \mathbf{S}_{(i)}$ , we can define  $\tilde{F}_{ip} = \mathbf{h}^{\top} \mathbf{s}_i^p$ , and rewrite our cost function in (7) as

$$\mathcal{L}(\mathbf{Z}, \mathbf{h}, \mathbf{V}) = \frac{\rho}{2} \sum_{p=1}^{P} \sum_{i=1}^{N} (Z_{ip} - F_{ip} + \mathbf{h}^{\top} \mathbf{s}_{i}^{p} + V_{ip})^{2} + \sum_{p=1}^{P} \sum_{i,j=1}^{N} (\mathbf{h}^{\top} \mathbf{s}_{i}^{p}) L_{ij} (\mathbf{h}^{\top} \mathbf{s}_{j}^{p}).$$

For updating  $\mathbf{h}$ , we set  $\nabla_h \mathcal{L} = 0$ , and after some algebraic manipulation, we obtain  $\mathbf{h}^{k+1} = -\mathbf{Y}^{-1}\mathbf{b}$ , where  $\mathbf{b} = \rho \sum_{p=1}^P \sum_{i=1}^N \mathbf{s}_i^p \mathbf{s}_i^p (Z_{ip}^{(k+1)} - F_{ip} + V_{ip}^{(k)})$  and  $\mathbf{Y} = \sum_{p=1}^P (2\sum_{i,j=1}^N \mathbf{s}_i^p L_{ij} \mathbf{s}_j^{p^\top} + \rho \sum_{i=1}^N \mathbf{s}_i^p \mathbf{s}_i^{p^\top})$ . In order to satisfy the constraint  $\mathbf{h}^\top \mathbf{h} = 1$ , we normalize  $\mathbf{h}^{k+1}$  by its norm  $||\mathbf{h}^{k+1}||_2$ .

3. V update: The Lagrangian multiplier can be updated using:

$$\mathbf{V}^{k+1} = \mathbf{V}^k + \rho(\mathbf{Z}^{k+1} - \mathbf{F} + \mathbf{U}\left(\sum_{t=0}^{T-1} h_t^{k+1} \mathbf{\Lambda}^t\right) \mathbf{U}^{\top} \mathbf{F}). \quad (8)$$

These three variables are updated until convergence.

# 3.3. Convergence

The optimization problem in (5) is convex, and the proposed solution is a two-block ADMM with convergence guarantees, which can be shown using approaches in [18]. Particularly, our problem is in the form of the general  $\ell_1$  regularized loss minimization problem [18], where l(h) in our case is the convex function  $\operatorname{tr}\left(\mathbf{F}^{\top}\mathbf{U}\left(\sum_{t=0}^{T-1}h_t\mathbf{\Lambda}^t\right)\mathbf{U}^{\top}\mathbf{L}\mathbf{U}\left(\sum_{t=0}^{T-1}h_t\mathbf{\Lambda}^t\right)\mathbf{U}^{\top}\mathbf{F}\right)$ , and g(z) is the  $\alpha||\mathbf{Z}||_1$  term. Therefore, our cost function satisfies the assumptions for the convergence proof provided in [18].

#### 3.4. Hub Node Scoring

Once we have the filtered graph signals, we use a scoring metric based on graph's local smoothness or variation defined as:

$$scores(i) = E(i) - \tilde{E}(i),$$
 (9)

where  $E(i) = \sum_{j=1}^{N} A_{ij} ||\mathbf{F}_{i} - \mathbf{F}_{j} \cdot ||^2$  and  $\tilde{E}(i) = \sum_{j=1}^{N} A_{ij} ||\tilde{\mathbf{F}}_{i} - \tilde{\mathbf{F}}_{j} \cdot ||^2$  are the local gradients at node i for the original and the filtered signals, respectively. Once the score is computed for all nodes  $i \in V$ , we identify the hub nodes as the ones with a z-score greater than 3, i.e., |z| > 3.

#### 4. RESULTS

#### 4.1. EEG Data and Pre-processing

EEG data is collected from a cognitive control-related error processing study where participants were performing a letter version of the speeded reaction Flanker task [19]. Each participant was presented with a string of five letters at each trial. Letters could be congruent (e.g., SSSSS) or incongruent stimuli (e.g., SSTSS) and the participants were instructed to respond to the center letter with a standard mouse. Each trial began with 35ms of flanking stimuli (e.g. SSSS), and followed by the target stimuli (e.g., SSSSS/SSTSS), which were presented for 100 ms (total presentation time is 135ms). Trials were followed by an inter-trial random interval ranging from 1200 to 1700 ms. The trials were conducted to study the Error-Related Negativity (ERN) after an error response, where each trial was one second long. Total number of trials was 480 in which the total number of error trials in different participants varied from 20 to 61.

The EEG was recorded using The ActiveTwo system (BioSemi, Amsterdam, The Netherlands). The international 10/20 system is followed for placement of 64 Ag–AgCl electrodes. The sampling frequency of the data was 512 Hz. After removal of the trials with artifacts, the Current Source Density (CSD) Toolbox [20] was employed to minimize the volume conduction.

As previous studies indicate increased synchronization associated with the ERN in the theta frequency band (4–7 Hz) and 25–75 ms time window [19, 21, 22], all analysis was performed for this time and frequency range. The average phase synchrony, i.e., PLV in (2), corresponding to the theta band and 25-75 ms time window was computed to construct the 64  $\times$  64 connectivity matrices for each subject. In order to obtain the graph signals, the EEG recordings for each subject and trial were first bandpass filtered within the  $\theta$  band and the time samples from 0-100 ms time window were extracted. These filtered and windowed time series are averaged across trials and used as the graph signals,  $\mathbf{F} \in \mathbb{R}^{64 \times 50}$  in GraFHub framework. In this paper, we consider data from 20 participants.  $^1$ 

## 4.2. Identification of Hub Nodes

We compare the prediction of hub nodes by GraFHub with three groups of methods that are commonly used for unsupervised outlier or hub detection. The first group is clustering methods, including One-Class Support Vector Machines (OCVSM) [23] and Robust Random Cut Forest (RRCForest) [24]. Both of these methods learn an anomaly region and classify the nodes based on whether the node resides within the region or not. As there are no prior training data, the methods are implemented in an unsupervised manner. The second group includes statistical methods, such as Principal Component Analysis (PCA) [25] and Local Outlier Factor (LOF) [26]. PCA identifies the normal subspace to reconstruct the data and finds anomalies using the reconstruction error. LOF uses data density to find anomalies based on neighbor distance. Both of these classes of methods are only applied directly to the attribute matrix without using the connectivity information. The final group is graph theoretic centrality measures such as the eigenvector and closeness centrality [4]. These metrics quantify a node's influence by how many other highly influential nodes it is connected to. Unlike our method, none of these methods utilizes both the adjacency matrix corresponding to the FCN and the EEG signal.

<sup>&</sup>lt;sup>1</sup>The code for GraFHub: https://github.com/a5sunbro/GraFHub

Participant number	GraFHub	OCVSM	PCA	LOF	RRCforest	Eigenvector	Closeness
1	P8	PO3, P10	POz, P8	P8, PO8	P8, PO8	P4, P10	P3, POz
2	FCz, P8, O2	FCz, TP8	POz, FCz	FCz, O2	FCz, O2	FT7, P8	CP3, P1
3	AF7	F2, P2	POz	P10, PO8	FCz, PO8	AF7, F4	C1, CP1
4	FT8, FCz	AF7, Fpz	POz	FC4, FCz	FT8, FCz	Iz, FT8	CP3, C2
5	P8, PO8	CP5, FZ		PO7, F4	PO7, F4	FT8, P10	P7, Cz
6	PO7	FC6, P4	Iz	F6, FC6	P6, O2	C5, Iz	C1, Cz
7	F6, P6	FC6, P4	Iz	F6, FC6	P6, O2	Fp1, AF8	C1, PO4
8	CPz, P6	POz	P5, PO3	FCz	Fp1, FCz	P4, P6	F7, FC1
9	FCz	Iz, Pz	POz, FCz	FT8, FCz	FT8, FCz	A7, AF8	PO3, Pz
10	FCz, P4	Pz, PO4	POz, FCz	FCz, P4	FCz, P4	Fz, F6	C3, Oz
11	FC4	AF7, C3		C5, FC4	FC4, P8	T7, P7	O1, P6
12	Fp1, FCz	CP3, FT8	FCz	Fpz, FCz	Fpz, FCz	Fp1, PO3	FC4, FC2
13	FCz	Iz, F6		FP1, FCz	Fp1, FCz	PO7, PO8	C1, Cz
14	C5	PO7, C2	POz, FCz	C5, FCz	F7, FCz	F7, F8	Fz, C2
15	FC2	PO3, Iz		FC2	Fp2, FC2	F5, O1	CPz, FC4
16	AF3, Fp2, FCz	C5, POz	FCz	FCz	FP2, FCz	AF3, F2	C3, C4
17	FCz	C1, CP4	FCz	FC1, FCz	FC1, FCz	C5, F8	PO3, F4
18	Cz	F1, C3	POz, FCz	FCz, Cz	FCz, Cz	AFz, FT8	FC2, P10
19	FCz, C2	P1, P10		FCz	F4, FCz	C2, CP2	PO3, Cz
20	AF7	CP1, Iz		AF7, F8	AF7, FP2	CP4, CP2	AF3, C5

**Table 1**: List of hub nodes detected by GraFHub and other methods for the 20 participants

Region	Frontal	Central	Parietal	Occipital	Temporal
Percentage of hubs	19%	45%	23%	10%	3%

Table 2: Percentage of hub nodes in different regions.

Table 1 lists the hub nodes identified by the different methods. Overall, our method's predictions are highly correlated with PCA, LOF, RRCForest, and Eigenvector Centrality. However, methods such as PCA are unable to detect hub nodes for certain participants. Moreover, for some of the participants, methods like OCSVM, PCA and eigenvector centrality detect electrodes such as Iz (over the inion) as the hub node whereas GraFHub mostly detects frontal-central regions as hubs.

Consistent with the role of medial frontal theta in coordinating widespread cortical networks during cognitive control, the most consistently identified hub nodes are in the frontal-central regions (see Table 2). Prior research [12, 27] indicates that error-related negativity amplitude response is highest over mid-frontocentral sites and mid-frontal scalp sites likely reflecting medial frontal cortex activity act as a strong "hub" for information flow.

## 4.3. Time Dynamics of Hub Nodes

Next, we evaluated the time dynamics of the identified hub nodes. Fig. 1 shows the topological map of the local total variation, i.e., the indicator of a hub node, as a function of time for a sample participant. From this figure, it can be seen that for the first 32 ms after the response, the local total variation is highest in the parietal-occipital regions as the stimulus is visual. From 32-64 ms after the response, this topomap gets more focused around FCz, corresponding to error monitoring. Similarly, Fig. 2 illustrates the anomaly score at the three hub nodes, FCz, P8 and O2, for the same participant. It can be seen that while this score is higher for the parietal and occipital electrodes for the first 40 ms, after this time point FCz becomes more prominent as expected indicating high mid-frontal activity during error-response.

## 5. CONCLUSIONS

In this paper, we introduced an unsupervised graph signal processing based approach to identify the hub nodes in FCNs. Unlike prior work which either considers the EEG waveforms or the functional connectivity matrices for hub node identification, the proposed method utilizes both the phase synchrony based connectivity matrix and the

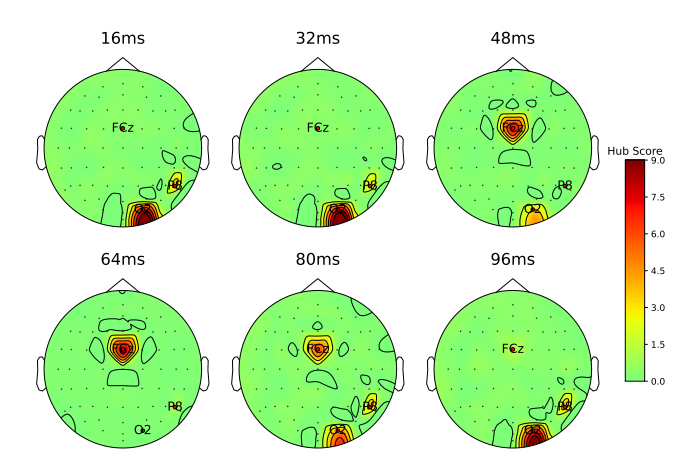
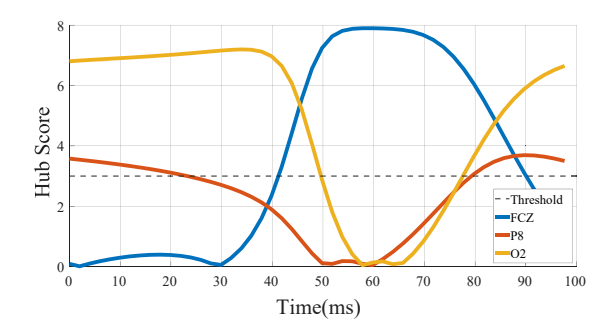


Fig. 1: Spatial distribution of hub score across time for participant



**Fig. 2**: Score of the hub nodes from participant 2 over time. Nodesmal with hub score (dashed line) over the threshold are predicted to be hubs.

EEG waveform. The hub detection problem is formulated as a filter design problem with the following two key assumptions: 1) the number of hub nodes is small, i.e., sparsity; 2) the hub nodes' signal amplitudes are different than their neighbors, i.e. heterophily. These two assumptions are incorporated in an optimization problem to learn the best graph filter to separate the hub nodes from normal nodes. A local total variation metric is introduced to quantify the 'hubness' of a node based on the filtered signals. The proposed framework is applied to a study of error-related negativity from 20 participants. The detected hub nodes are compared to other commonly used hub identification and anomaly detection methods. It is seen that the proposed method consistently identifies hub nodes in the mid-frontal central and parietal-occipital regions. We also illustrated the ability of the method to track the hub node's score as a function of time highlighting the correlation between the peak of hub score with ERN amplitude. Future work will focus on improving this method by extending the framework for joint hub node identification across a group of subjects or modalities.

## 6. COMPLIANCE WITH ETHICAL STANDARDS

The study was designed following the experimental protocol and guidelines approved by the Institutional Review Board (IRB) of the

Michigan State University (IRB: LEGACY13-144). The data acquisition was performed following the guidelines and regulations established by this protocol. Written and informed consent was collected from each participant before data collection.

#### 7. ACKNOWLEDGEMENTS

This work was supported in part by the NSF under CCF-2211645 and CCF-2312546.

## 8. REFERENCES

- [1] Ed Bullmore and Olaf Sporns, "Complex brain networks: graph theoretical analysis of structural and functional systems," *Nature reviews neuroscience*, vol. 10, no. 3, pp. 186–198, 2009.
- [2] Olaf Sporns, Christopher J Honey, and Rolf Kötter, "Identification and classification of hubs in brain networks," *PloS one*, vol. 2, no. 10, pp. e1049, 2007.
- [3] Jonathan D Power, Bradley L Schlaggar, Christina N Lessov-Schlaggar, and Steven E Petersen, "Evidence for hubs in human functional brain networks," *Neuron*, vol. 79, no. 4, pp. 798–813, 2013.
- [4] Martijn P Van den Heuvel and Olaf Sporns, "Network hubs in the human brain," *Trends in cognitive sciences*, vol. 17, no. 12, pp. 683–696, 2013.
- [5] Weiyu Huang, Thomas AW Bolton, John D Medaglia, Danielle S Bassett, Alejandro Ribeiro, and Dimitri Van De Ville, "A graph signal processing perspective on functional brain imaging," *Proceedings of the IEEE*, vol. 106, no. 5, pp. 868–885, 2018.
- [6] Maria Giulia Preti and Dimitri Van De Ville, "Decoupling of brain function from structure reveals regional behavioral specialization in humans," *Nature communications*, vol. 10, no. 1, pp. 4747, 2019.
- [7] Mathilde Ménoret, Nicolas Farrugia, Bastien Pasdeloup, and Vincent Gripon, "Evaluating graph signal processing for neuroimaging through classification and dimensionality reduction," in 2017 IEEE Global Conference on Signal and Information Processing (GlobalSIP). IEEE, 2017, pp. 618–622.
- [8] Yixin Liu, Zhao Li, Shirui Pan, Chen Gong, Chuan Zhou, and George Karypis, "Anomaly detection on attributed networks via contrastive self-supervised learning," *IEEE transactions* on neural networks and learning systems, vol. 33, no. 6, pp. 2378–2392, 2021.
- [9] Tong Zhao, Chuchen Deng, Kaifeng Yu, Tianwen Jiang, Daheng Wang, and Meng Jiang, "Gnn-based graph anomaly detection with graph anomaly loss," in *The Second International Workshop on Deep Learning on Graphs: Methods and Applications*, 2020, pp. 1–7.
- [10] Muhammet Balcilar, Renton Guillaume, Pierre Héroux, Benoit Gaüzère, Sébastien Adam, and Paul Honeine, "Analyzing the expressive power of graph neural networks in a spectral perspective," in *Proceedings of the International Conference on Learning Representations (ICLR)*, 2021.
- [11] Jianheng Tang, Jiajin Li, Ziqi Gao, and Jia Li, "Rethinking graph neural networks for anomaly detection," in *International Conference on Machine Learning*. PMLR, 2022, pp. 21076–21089.

- [12] Selin Aviyente, Edward M Bernat, Westley S Evans, and Scott R Sponheim, "A phase synchrony measure for quantifying dynamic functional integration in the brain," *Human Brain Mapping*, vol. 32, no. 1, pp. 80–93, 2011.
- [13] Leon Cohen, *Time-frequency analysis*, vol. 778, Prentice hall New Jersey, 1995.
- [14] A Rihaczek, "Signal energy distribution in time and frequency," *IEEE Transactions on information Theory*, vol. 14, no. 3, pp. 369–374, 1968.
- [15] Santiago Segarra, Antonio G Marques, and Alejandro Ribeiro, "Optimal graph-filter design and applications to distributed linear network operators," *IEEE Transactions on Signal Process*ing, vol. 65, no. 15, pp. 4117–4131, 2017.
- [16] Ziwei Chai, Siqi You, Yang Yang, Shiliang Pu, Jiarong Xu, Haoyang Cai, and Weihao Jiang, "Can abnormality be detected by graph neural networks?," in *Proceedings of the Twenty-Ninth International Joint Conference on Artificial Intelligence (IJCAI)*, Vienna, Austria, 2022, pp. 23–29.
- [17] Neal Parikh, Stephen Boyd, et al., "Proximal algorithms," *Foundations and trends*® *in Optimization*, vol. 1, no. 3, pp. 127–239, 2014.
- [18] S. Boyd, N. Parikh, E. Chu, B. Peleato, and J. Eckstein, "Distributed optimization and statistical learning via the alternating direction method of multipliers," vol. 3, no. 1, pp. 1–122, Jan. 2011.
- [19] Jason R Hall, Edward M Bernat, and Christopher J Patrick, "Externalizing psychopathology and the error-related negativity," *Psychological science*, vol. 18, no. 4, pp. 326–333, 2007.
- [20] Craig E Tenke and Jürgen Kayser, "Generator localization by current source density (csd): implications of volume conduction and field closure at intracranial and scalp resolutions," *Clinical neurophysiology*, vol. 123, no. 12, pp. 2328–2345, 2012.
- [21] James F Cavanagh and Michael J Frank, "Frontal theta as a mechanism for cognitive control," *Trends in cognitive sciences*, vol. 18, no. 8, pp. 414–421, 2014.
- [22] Marcos Bolanos, Edward M Bernat, Bin He, and Selin Aviyente, "A weighted small world network measure for assessing functional connectivity," *Journal of neuroscience* methods, vol. 212, no. 1, pp. 133–142, 2013.
- [23] Young-Sik Choi, "Least squares one-class support vector machine," *Pattern Recognition Letters*, vol. 30, no. 13, pp. 1236– 1240, 2009.
- [24] Matthew D Bartos, Abhiram Mullapudi, and Sara C Troutman, "rrcf: Implementation of the robust random cut forest algorithm for anomaly detection on streams," *Journal of Open Source Software*, vol. 4, no. 35, pp. 1336, 2019.
- [25] Markus Ringnér, "What is principal component analysis?," Nature biotechnology, vol. 26, no. 3, pp. 303–304, 2008.
- [26] Juozas Auskalnis, Nerijus Paulauskas, and Algirdas Baskys, "Application of local outlier factor algorithm to detect anomalies in computer network," *Elektronika ir Elektrotechnika*, vol. 24, no. 3, pp. 96–99, Jun. 2018.
- [27] Michael X Cohen, "Error-related medial frontal theta activity predicts cingulate-related structural connectivity," *Neuroimage*, vol. 55, no. 3, pp. 1373–1383, 2011.